Microwave Absorption Properties of Carbon Nanocoils Coated with Highly Controlled Magnetic Materials by Atomic Layer Deposition

Guizhen Wang,[†,‡,§] Zhe Gao,[†] Shiwei Tang,[⊥] Chaoqiu Chen,[†] Feifei Duan,[†] Shichao Zhao,[†,‡] Shiwei Lin,[§] Yuhong Feng,[§] Lei Zhou,[⊥] and Yong Qin[†,*]

[†]State Key Laboratory of Coal Conversion, Institute of Coal Chemistry, Chinese Academy of Sciences, Taiyuan 030001, People's Republic of China, [‡]University of Chinese Academy of Sciences, Beijing 100039, People's Republic of China, [§]Key Laboratory of Chinese Education Ministry for Tropical Biological Resources, Hainan University, Haikou 570228, People's Republic of China, and [⊥]State Key Laboratory of Surface Physics and Key Laboratory of Micro and Nano Photonic Structures (Ministry of Education), Fudan University, Shanghai 200433, People's Republic of China

ABSTRACT In this work, atomic layer deposition is applied to coat carbon nanocoils with magnetic Fe_3O_4 or Ni. The coatings have a uniform and highly controlled thickness. The coated nanocoils with coaxial multilayer nanostructures exhibit remarkably improved microwave absorption properties compared to the pristine carbon nanocoils. The enhanced absorption ability arises from the efficient complementarity between complex permittivity and permeability, chiral morphology, and multilayer structure of the products. This method can be extended to exploit other composite materials benefiting from its convenient control of the impedance matching and combination of dielectric—magnetic multiple loss mechanisms for microwave absorption applications.

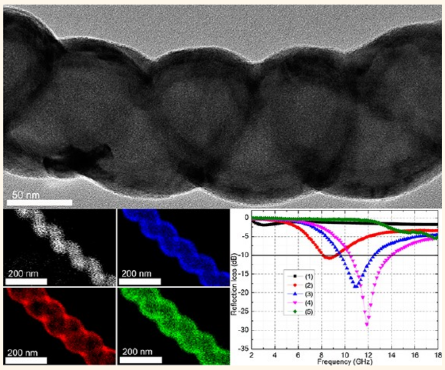

KEYWORDS: atomic layer deposition · carbon nanocoils · core—shell nanostructures · magnetic materials · microwave absorption

Chiral materials are superior for constructing highly efficient microwave absorbers with light weight, wide absorption frequency range, and strong absorption ability because of an additional more adjustable chiral parameter besides the complex permittivity and permeability leading to optical rotation and circular dichroism from the cross-coupling effect between the magnetic and electric fields.[1−4] Previous studies related to chiral materials mostly focused on metallic springs embedded in a low-loss matrix. Such materials are difficult for wide application owing to large size, high density, and strong reflection. Carbon nanocoil (CNC) is a representative chiral material with many advantages such as light weight, high electrical conductivity, and good stability, thus much attention has been attached to its application in thin and broad-band absorbers.[5,6] However, excellent electromagnetic (EM) wave absorption usually results from efficient complementarities between the relative permittivity and permeability in materials. Only dielectric loss or magnetic loss leads to a weak EM impedance matching. Single-component CNCs show dominantly dielectric loss and very low magnetic loss due to weak magnetic properties, which hampers their applications. Therefore, it is quite necessary to incorporate them with magnetic materials, to improve impedance matching, increase the magnetic loss, broaden the absorption bandwidth, and enhance absorption intensity. Traditional electroless deposition methods[7] to incorporate CNCs with magnetic coatings have no good control over coating quality and uniform thickness because the CNCs have small diameters, low chemical reactivity, and particularly large surface curvature.

Atomic layer deposition (ALD) is a powerful technique for conformal coating on high aspect ratio materials with outstanding

* Address correspondence to qinyong@sxicc.ac.cn.

Received for review October 6, 2012 and accepted November 21, 2012.

10.1021/nn304630h

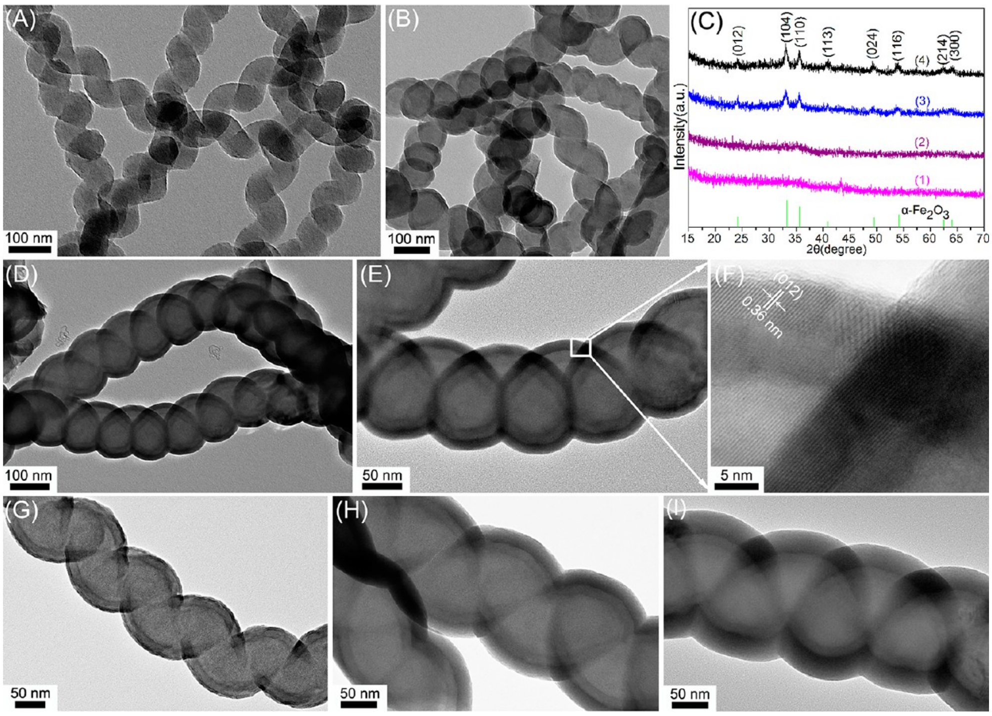

Figure 1. (A) TEM image of CNCs. (B) TEM image of Al_2O_3/CNC obtained by applying 100 ALD cycles of Al_2O_3 deposition. (C) XRD patterns of Fe_2O_3/Al_2O_3/CNC nanocomposites obtained by applying 100 ALD cycles of Al_2O_3 deposition and then 600 (1), 1200 (2), 2400 (3), and 3600 (4) cycles of Fe_2O_3 deposition, respectively. (D,E) Low-magnification TEM and (F) HRTEM images of Fe_2O_3/Al_2O_3/CNC structures obtained by applying 100 ALD cycles of Al_2O_3 and then 1200 cycles of Fe_2O_3 deposition. (G–I) TEM images of Fe_2O_3/Al_2O_3/CNC structure obtained by applying 100 ALD cycles of Al_2O_3 and then 600, 2400, and 3600 cycles of Fe_2O_3 deposition, respectively.

advantages including precise thickness control, excellent uniformity, and sharp interfaces.[8−10] At present, a large variety of materials are available by ALD, including metals, oxides, nitrides, sulfides, phosphates, *etc*. In particular, some high dielectric materials (Al_2O_3[11] and ZrO_2[12]) and magnetic materials (Fe_3O_4,[13] Ni,[14−16] Co,[15,16] and $NiFe_2O_4$[17]) can be produced by ALD, which is helpful to intentionally design excellent microwave absorbers by carefully adjusting the materials' complex permittivity and permeability.

Herein, we report the synthesis of Fe_3O_4/Al_2O_3/CNC and Ni/Al_2O_3/CNC coaxial multilayer nanostructures by ALD to demonstrate a general strategy for the preparation of highly efficient microwave absorbers. The microwave absorption properties of as-prepared magnetic CNCs were investigated in terms of complex permittivity and permeability. Our results show that these magnetic CNCs with highly controlled coating thickness, good conformality, and multilayer core−shell nanostructures have a significant reduction in EM reflection loss (RL) and confirm that ALD can also be extended to exploit other composite materials benefiting from its convenient control of the impedance matching and combination of dielectric−magnetic multiple loss mechanisms for microwave absorption applications.

RESULTS AND DISCUSSION

Figure 1A displays a representative transmission electron microscopy (TEM) image of the starting CNCs used in this study. The CNCs have a diameter of approximately 100 nm and an average length of 10 μm. They are tightly coiled and have very uniform coil pitches and coil diameters. Usually, magnetic films can be synthesized by the deposition of metal oxides (Fe_2O_3, NiO) and subsequent reduction under hydrogen atmosphere. In previous reports, O_3 was proved to be favorable for ALD of metal oxides to obtain a highly conformal and dense thin film.[18−20] Furthermore, the use of O_3 enables growth over a much wider temperature range. Unfortunately, O_3 will lead to a strong thermal oxidation of CNCs. For this reason, protection of CNCs by depositing thin layers of oxidation barrier coatings onto their surfaces is considered as an effective strategy.[21] As observed from the TEM image shown in Figure 1B, by applying 100 ALD cycles for Al_2O_3 deposition, a uniform Al_2O_3 film with a thickness of about 12 nm is coated on the CNCs. High-magnification TEM and high-resolution TEM (HRTEM) analyses (Supporting Information Figure S1) further reveal the amorphous nature of the Al_2O_3 shells.

The advantages of ALD enable us to prepare coaxial multilayer structures by changing precursors without treating the samples during the deposition interval. Therefore, the as-prepared Al_2O_3/CNCs can be sequentially deposited with Fe_2O_3 layers by using ferrocene ($FeCp_2$) and O_3 as precursors. Figure 1C displays XRD patterns of Al_2O_3/CNCs coated by 600, 1200, 2400, and 3600 ALD cycles of Fe_2O_3 deposition, respectively.

There are no clear diffraction peaks of Fe_2O_3 for products after 600 and 1200 ALD cycles of Fe_2O_3 deposition, which is probably due to the low content of Fe_2O_3 in composites. When the ALD cycles of Fe_2O_3 are increased to 2400 or 3600 cycles, distinct diffraction peaks are observed and can be indexed to those of rhombohedral phase of α-Fe_2O_3 with the lattice parameters of a = 5.032 Å and c = 13.733 Å, which are consistent with the reported values (Joint Committee on Powder Diffraction Standards (JCPDS), powder diffraction file no. 89-0599). No characteristic peaks of impurities, such as γ-Fe_2O_3, Fe_3O_4, or FeO, can be detected, suggesting that the strong oxidation ability of O_3 in the present system likely precludes the mixing of incompletely oxidized forms of iron and induces higher oxidation states of iron.[19,22]

TEM and HRTEM images provide insights into the morphology and detailed structure of the as-prepared Fe_2O_3/Al_2O_3/CNC. Figure 1D,E shows low-magnification TEM images of Fe_2O_3/Al_2O_3/CNC obtained by applying 100 ALD cycles of Al_2O_3 and then 1200 cycles of Fe_2O_3 deposition. The formed Fe_2O_3/Al_2O_3/CNC core–shell structure is clearly visible due to their different contrasts. The Fe_2O_3 shells are about 12 nm thick. The HRTEM image clearly shows the lattice fringes of Fe_2O_3 shells with a rhombohedral structure (Figure 1F), in agreement with the XRD data. The interplanar spacing is about 0.36 nm, corresponding to the (012) crystal plane of rhombohedral phase Fe_2O_3. ALD can easily achieve the Fe_2O_3 thickness control by changing the deposition cycle number. Figure 1G–I shows the TEM images of Fe_2O_3/Al_2O_3/CNC obtained by applying 600, 2400, and 3600 ALD cycles of Fe_2O_3 deposition, respectively. All Fe_2O_3/Al_2O_3/CNCs display clear multilayer core–shell structures, and the thickness of Fe_2O_3 shells clearly increases with the increase of ALD cycles. It amounts to about 6, 24, and 36 nm Fe_2O_3 shells, respectively, which corresponds to a growth rate of about 0.1 Å per cycle. Low-magnification TEM (Supporting Information Figure S2) images further confirm that these samples also have a uniform thickness and multilayer helical morphology, and the lattice fringes from HRTEM images (Supporting Information Figure S3) reveal the feature of rhombohedral phase Fe_2O_3. Energy-dispersive X-ray spectroscopy (EDX) (Supporting Information Figure S4) made on the as-synthesized Fe_2O_3/Al_2O_3/CNCs from different ALD cycles of Fe_2O_3 indicates the existence of Fe, Al, C, and O elements and the increased Fe atom ratio with the increase of ALD cycles.

The α-Fe_2O_3 can be readily converted to magnetic Fe_3O_4 by a reduction process. Fe_3O_4/Al_2O_3/CNC core–shell structures were obtained by annealing Fe_2O_3/Al_2O_3/CNCs at 450 °C for 2 h under a mixture of N_2/H_2 flow in a tube furnace. The structure and morphology of as-prepared Fe_3O_4/Al_2O_3/CNCs were investigated by means of XRD and TEM. Figure 2A shows the XRD pattern of the Fe_3O_4/Al_2O_3/CNC composites (100 cycles of Al_2O_3, 1200 cycles of Fe_2O_3, and then a hydrogen reduction). All peaks indicated by Miller indices come from the face-centered cubic crystal structure of Fe_3O_4 according to JCPDF card no. 01-1111. The relative strong and sharp diffraction peaks indicate the good crystallinity of the as-synthesized Fe_3O_4. Typical TEM image (Figure 2B) shows that the helical morphology in Fe_3O_4/Al_2O_3/CNC composites is still well preserved after the reduction process. The inset in Figure 2B exhibits a corresponding selected area electron diffraction (SAED) pattern recorded on an individual nanocoil. Several rings can be assigned to diffraction planes of the cubic phase of Fe_3O_4, revealing the polycrystalline structure. A high-magnification TEM image (Figure 2C) shows that Fe_3O_4/Al_2O_3/CNC retains clear three-layer core–shell structure. In comparison to Fe_2O_3/Al_2O_3/CNC, the Fe_3O_4 shells are also about 12 nm thick, indicating a negligible variation in shell thickness due to only approximately 3.33% shrinkage from the release of oxygen anions after reduction of α-Fe_2O_3 to Fe_3O_4. The HRTEM image highlights the well-defined crystalline lattice spacing of 0.30 and 0.49 nm, which can be indexed as (220) and (111) crystal planes of Fe_3O_4 (Figure 2D), respectively. The STEM characterization and elemental maps of an individual Fe_3O_4/Al_2O_3/CNC are displayed in Figure 2E–J. The line scan analysis in Figure 2E reveals the profile of C, Al, Fe, and O atoms across the helical section, indicating an apparent three-layer core–shell structure. The elemental maps of C, Al, Fe, O, and their overlap further demonstrate that the three elements, Al, Fe, and O, are evenly distributed on the surface of CNCs and maintain a consistent helical morphology. In addition, magnetic CNCs with 6, 24, and 36 nm Fe_3O_4 coating have also been obtained by the same reduction process (Supporting Information Figures S5 and S6).

In order to investigate the microwave absorption properties of the products, specimens were prepared by uniformly mixing 25 wt % uncoated or coated nanocoils with paraffin and pressing the mixture into a cylindrical shape. Then the cylinder was cut into a toroid of 7.00 mm outer diameter and 3.04 mm inner diameter for measurement. The complex permittivity and permeability of the composites were measured by using the transmission/reflection coaxial line method.[23,24] It should be noted that the measured permittivity and permeability represent the properties of the mixture of pristine or coated nanocoils because the microwaves cannot resolve each nanocoil and observe an effective medium (mixture) since the smallest microwave wavelength used is about 17 mm (18 GHz), while the diameter of the nanocoils is about 100 nm.

The reflection loss (RL) coefficients of these materials were calculated by using the measured relative complex permittivity and permeability values. According to transmission line theory, the RL coefficient (dB) of

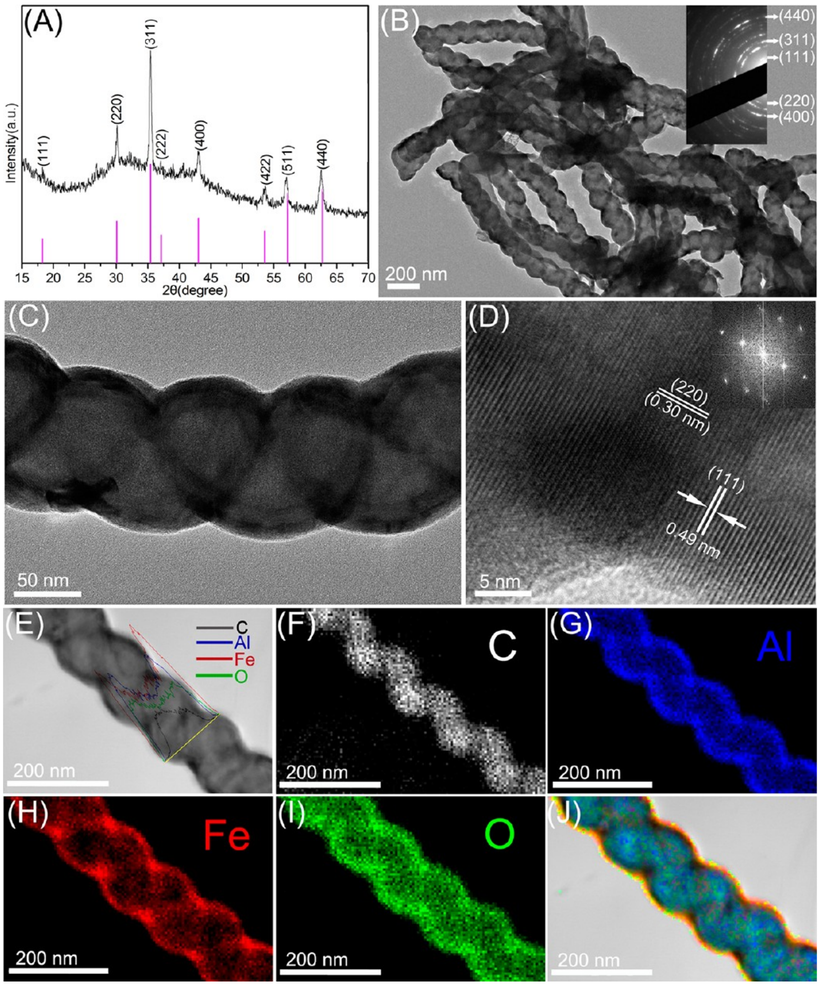

Figure 2. (A) XRD pattern of the Fe_3O_4/Al_2O_3/CNCs (by 100 cycles of Al_2O_3, 1200 cycles of Fe_2O_3, and then a hydrogen reduction). (B) TEM image. (C) TEM and (D) HRTEM images of an individual Fe_3O_4/Al_2O_3/CNC. (E) STEM characterization of the Fe_3O_4/Al_2O_3/CNC with line scan profile across the helical section and corresponding elemental mapping images of (F) C, (G) Al, (H) Fe, (I) O, and (J) their overlap.

electromagnetic wave (normal incidence) at the surface of a single-layer material backed by a perfect conductor at a given frequency and layer thickness can be defined with the following equations:[25−28]

$$Z_{in} = Z_0(\mu_r/\varepsilon_r)^{1/2}\tanh[j(2\pi fd/c)(\mu_r\varepsilon_r)^{1/2}] \qquad (1)$$

$$RL = 20\log|(Z_{in} - Z_0)/(Z_{in} + Z_0)| \qquad (2)$$

where Z_{in} is the input impedance of the absorber, Z_0 the impedance of free space, μ_r the relative complex permeability, ε_r the complex permittivity, f the frequency of microwaves, d the thickness of the absorber, and c the velocity of light. A RL value of −10 dB is comparable to 90% microwave absorption. In general, materials with RL values of less than −10 dB absorption are considered to be suitable EM wave absorbers.

Figure 3A shows a comparison of calculated RL curves in the frequency range of 2−18 GHz for the product/paraffin composites with a thickness of 2 mm. It can be found that the RL properties of pristine CNCs are expected mainly from dielectric loss, with a minimum RL of −1.97 dB. Compared to the pristine CNCs, the RL performances toward EM waves of magnetic CNCs are enhanced substantially. The minimum RL of Fe_3O_4/Al_2O_3/CNCs with 6, 12, 24, and 36 nm Fe_3O_4 shells (mentioned as 6, 12, 24, and 36-Fe_3O_4/Al_2O_3/CNCs, hereafter) are −10.7, −18.4, −28.3, and −5.5 dB at 8.8, 10.9, 11.9, and 17.7 GHz, respectively. The microwave absorption values less than −10 dB for 12-Fe_3O_4/Al_2O_3/CNCs and 24-Fe_3O_4/Al_2O_3/CNCs are in the ranges of 9.6−12.4 and 10.5−14.0 GHz, respectively. In addition, the frequency related to minimum RL can be modulated by increasing the thickness of Fe_3O_4 shells, and the absorption peaks shift to higher frequency accompanied by the attenuation at lower frequency bands. Such a phenomenon was also observed in a previous report about Ni/PPy composites by altering the content of PPy.[29] To reveal in detail the influences of thickness on the absorption properties, three-dimensional RL values of 6, 12, and 24-Fe_3O_4/Al_2O_3/CNCs are shown in Figure 3B−D. The minimum RL reaches −40.3 dB for 24-Fe_3O_4/Al_2O_3/CNCs with a

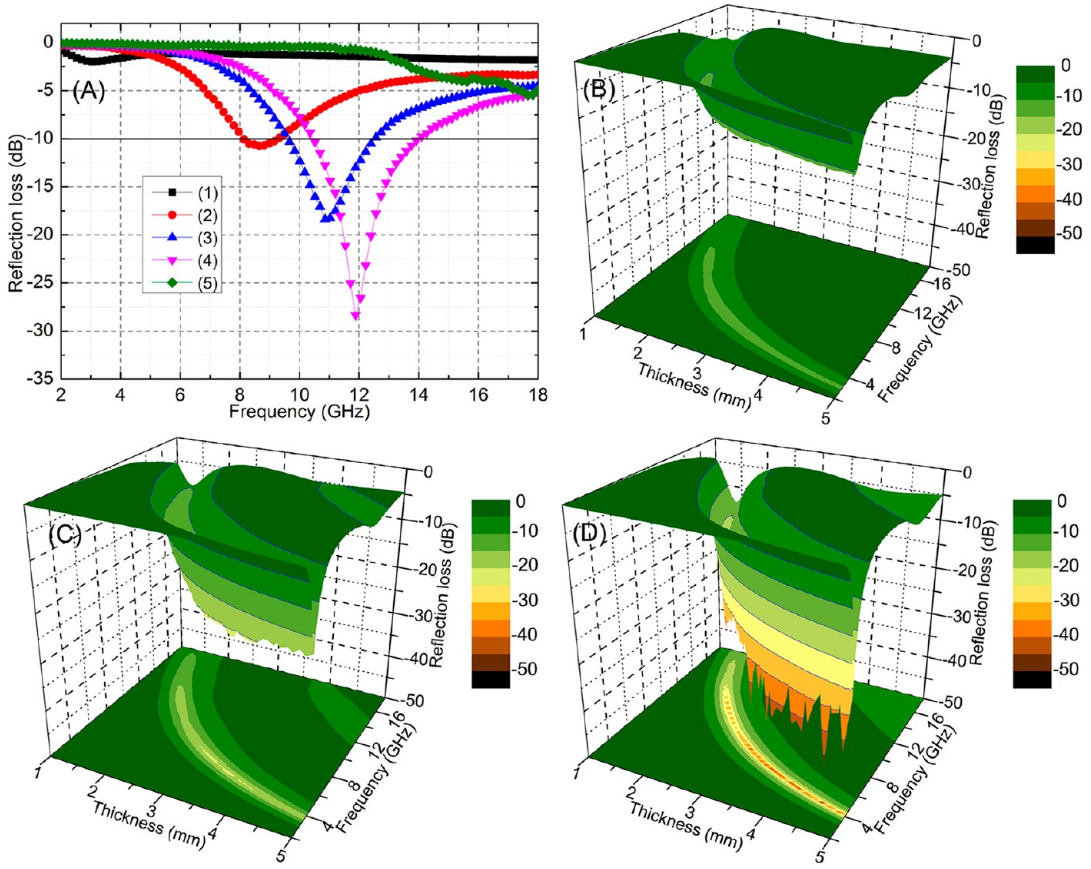

Figure 3. Microwave absorption properties of the products calculated by using the measured relative complex permittivity and permeability values according to transmission line theory. (A) Microwave RL curves of the product/paraffin composites with a thickness of 2 mm in the frequency range of 2−18 GHz: (1) pristine CNCs, (2) 6-Fe_3O_4/Al_2O_3/CNCs, (3) 12-Fe_3O_4/Al_2O_3/CNCs, (4) 24-Fe_3O_4/Al_2O_3/CNCs, and (5) 36-Fe_3O_4/Al_2O_3/CNCs. Three-dimensional representations of RL of (B) 6-Fe_3O_4/Al_2O_3/CNCs, (C) 12-Fe_3O_4/Al_2O_3/CNCs, and (D) 24-Fe_3O_4/Al_2O_3/CNCs.

thickness of 3.1 mm, −21.5 dB with a thickness of 3.6 mm for 12-Fe_3O_4/Al_2O_3/CNCs, and −11.8 dB with a thickness of 3.1 mm for 6-Fe_3O_4/Al_2O_3/CNCs, respectively. Moreover, it can be observed that the absorption bandwidth with RL below −20 dB is obtained in the frequency range of 4.1−13.4 GHz for 24-Fe_3O_4/Al_2O_3/CNCs with a thickness of 1.8−5 mm. All of these values are evidently improved relative to the pristine CNCs, demonstrating that Fe_3O_4/Al_2O_3/CNCs with a compatible thickness of Fe_3O_4 shells can greatly ameliorate their microwave absorbing performance.

In general, the reflection and attenuation properties of EM wave absorbers depend on the matching frequency, layer thickness of absorbers, and the relative complex permeability and permittivity, which are determined by their nature, shape, size, and microstructure.[30,31] In the present work, there are three reasons for the high efficient microwave absorption properties of Fe_3O_4/Al_2O_3/CNCs. First, the improvement in microwave absorption originates from the efficient combination of coaxial multilayer structures of magnetic CNCs. According to transmission line theory, the RL would be improved when the dielectric contribution matches the magnetic contribution based on the requirement of the input impedance.[26] The complex permittivity real part (ε'), permittivity imaginary part (ε''), permeability real part (μ'), and permeability imaginary part (μ'') of the CNC-paraffin and Fe_3O_4/Al_2O_3/CNC-paraffin were investigated in the frequency range of 2−18 GHz (Figure 4). The pristine CNCs show negligible permeability due to the lack of magnetic composition and very high ε' and ε'' values from 182.1 to 15.6 and from 120.4 to 54.0, respectively. This means that the magnetic loss and the dielectric loss are out of balance in this case, inducing poor EM wave absorption. By coating with Fe_3O_4 shells, the CNCs can be endued with magnetism, and the corresponding saturation magnetizations, coercivities, and remnant magnetizations increase appropriately with the increasing Fe_3O_4 thickness (Figure 5). The magnetic CNCs show reduced complex permittivity and increased complex permeability compared to pristine CNCs. Moreover, it is interesting that the trend on complex permittivity has also changed. The ε' values continue to decline, but ε'' values have a slight increase in the whole frequency range. Such changes are beneficial for the efficient complementarity between the permittivity and permeability. Therefore, in the

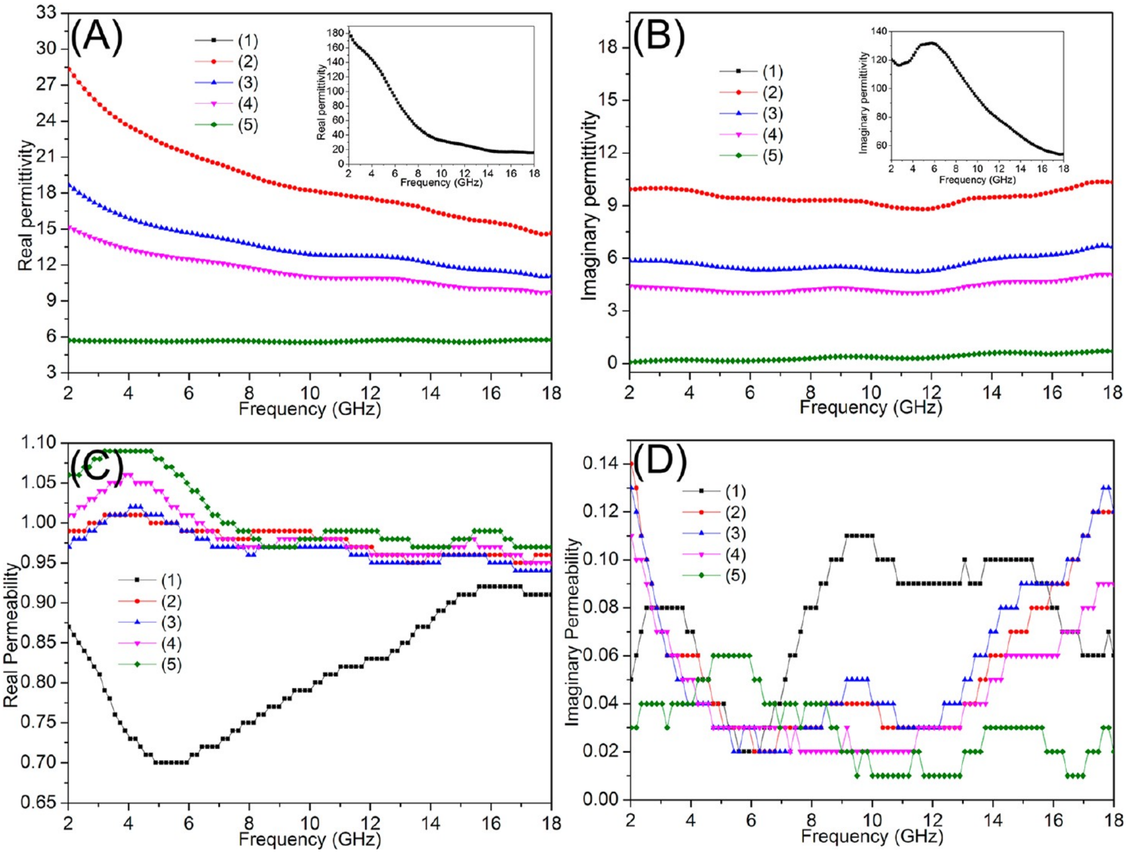

Figure 4. Measured frequency dependence of (A) real and (B) imaginary parts of complex permittivity and (C) real and (D) imaginary parts of permeability: (1) pristine CNCs, (2) 6-Fe_3O_4/Al_2O_3/CNCs, (3) 12-Fe_3O_4/Al_2O_3/CNCs, (4) 24-Fe_3O_4/Al_2O_3/CNCs, and (5) 36-Fe_3O_4/Al_2O_3/CNCs.

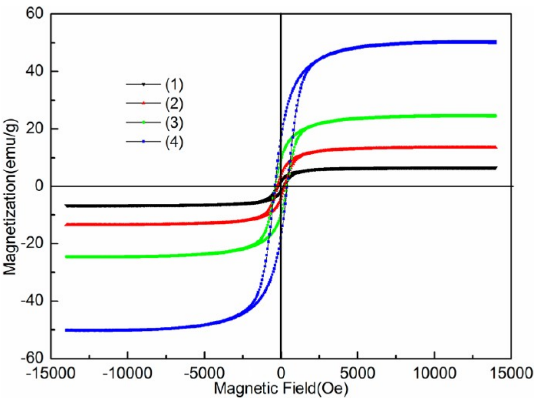

Figure 5. Hysteresis loops of magnetic CNCs measured at 300 K: (1) 6-Fe_3O_4/Al_2O_3/CNCs, (2) 12-Fe_3O_4/Al_2O_3/CNCs, (3) 24-Fe_3O_4/Al_2O_3/CNCs, and (4) 36-Fe_3O_4/Al_2O_3/CNCs.

cases of the 6−24-Fe_3O_4/Al_2O_3/CNCs, with the increase of Fe_3O_4 thickness, a better EM impedance matching is realized due to the combination of dielectric loss of CNCs, the magnetic loss of Fe_3O_4, and their special core−shell structure. However, for the 36-Fe_3O_4/Al_2O_3/CNCs, excessively low ε'' is caused by the too thick Fe_3O_4 coatings, thus leading to reduced absorption abilities. Second, Fe_3O_4/Al_2O_3/CNC is a type of representative chiral material with nanocoiling morphology and thus expected to have different interactions with the EM wave from nonchiral materials. When EM wave flows along the helix, Fe_3O_4/Al_2O_3/CNCs act as multiple nanosolenoids and inductive electromotive force is generated, resulting in induced current in the helix according to Faraday's law.[32] However, this current encounters the difficulty of transmitting due to the insulated Al_2O_3 layer on the outside of the CNCs. So the eddy current loss is considered to have an important contribution to the improved microwave RL. The eddy current loss is related to the diameter of the nanoparticle (d) and electric conductivity (σ), which can be expressed by the equation $\mu'' \approx 2\pi\mu_0(u')^2\sigma d^2 f/3$, where μ_0 is the permeability of vacuum. According to the equation, if the magnetic loss only originates from the eddy current loss, the values of $\mu''(u')^{-2}f^{-1}$ should be constant when the frequency is changed. In our work, the $\mu''(u')^{-2}f^{-1} = 2\pi\mu_0\sigma d^2/3$ remains approximately constant when $f > 4$ GHz (Supporting Information Figure S7), which confirms that magnetic loss is caused mainly by the eddy current loss. Moreover, when the EM wave irradiates the helix, not only does it produce a magnetic polarization along the axis but also it produces an electric polarization because some of EM wave flows parallel to the axis.[32,33] The effective polarization forms planar and/or circularly polarized waves, right-handed or left-handed, and are also reflected or

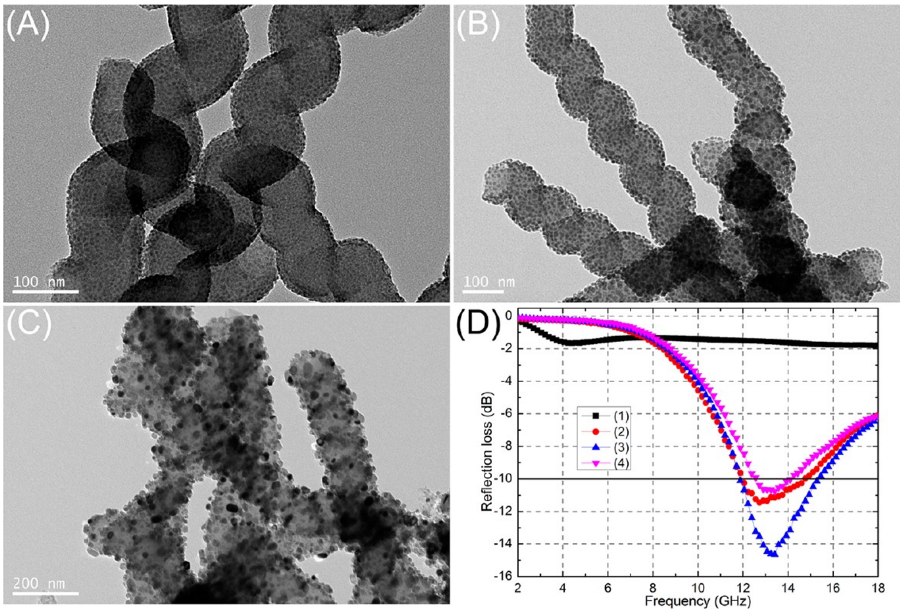

Figure 6. TEM images of Ni/Al_2O_3/CNCs obtained by applying (A) 400, (B) 800, and (C) 1600 cycles of NiO deposition and then a hydrogen reduction process. (D) Microwave RL curves of the product/paraffin composites with a thickness of 1.5 mm: (1) pristine CNCs, (2) 4.7-Ni/Al_2O_3/CNCs, (3) 8.9-Ni/Al_2O_3/CNCs, and (4) 18.3-Ni/Al_2O_3/CNCs.

dispersed, and thus are then sharply attenuated. Third, it has been reported that core–shell structured composites show great potential as microwave absorbers with lower RL and wider absorption frequency range than single-component absorbers due to effective interfaces and its associated relaxation loss.[34−39] Obviously, Fe_3O_4/Al_2O_3/CNC is a clear multilayer heterogeneous system, in which interfacial polarization of the free charge on the conductor–insulator may be important and will give rise to significant loss.

In this work, the used carbon nanocoils were synthesized by the same method reported previously.[40] These nanocoils exhibit an absolute symmetric growth mode.[41] There are always two nanocoils grown on a single copper nanoparticle. Moreover, the two nanocoils always have absolute opposite coiled/helical directions and identical lengths. For permittivity and permeability measurement, these uncoated or coated nanocoils are randomly and uniformly dispersed in paraffin, so there should be no alignment in the mixture considering that their sizes (micrometer in length and nanometer in diameter) are much smaller than those (millimeter) of the cylinder for measurement. Therefore, it can be inferred that the mixture should be a macroscopic racemic/isotropic effective medium due to the identical contents of left- and right-handed coiled nanocoils and thus show no polarization and rotation angles.[42] The permittivity and permeability will not be direction-dependent in terms of the angle of incident microwave. Moreover, the absorption will not depend on the polarization of incident waves.

We also performed preliminary theoretical calculation with effective medium theory for the complex permittivity and permeability of these materials. Considering that an incident wave is not sensitive to particles or structures with sizes that are smaller than a sensing wavelength, in this work, the EM parameters of composite materials can be calculated by the Maxwell–Garnett (M–G) equation (see Supporting Information). The calculated results reveal that the real parts of permittivity exhibit a similar tendency compared with the measured values, while the imaginary parts of permittivity are not very consistent with the experimental results (Supporting Information Figure S8). A large deviation can be found for the complex permeability. Possibly the reason is that M–G theory describes the inclusions as spherical particles employing averaged demagnetization factor. Actually, the effective EM parameters of the composites are affected greatly by the shape distribution of the inclusions. Further work is necessary for more accurate calculation with the one-dimensional structure and helical morphology of the nanocoils being considered.

For the present work, the same procedure was also applied to the synthesis of Ni/Al_2O_3/CNCs. TEM images (Supporting Information Figure S9) show that NiO/Al_2O_3/CNCs with dense NiO films can be obtained by applying 400, 800, and 1600 ALD cycles. It is interesting that such NiO films can be converted to uniform Ni nanoparticle films after a hydrogen reduction process. As shown in Figure 6A–C, the average diameters of Ni nanoparticles measured by TEM are 4.7, 8.9, and 18.3 nm corresponding to 400, 800, and 1600 cycles of NiO deposition, respectively (mentioned as 4.7-, 8.9-, and 18.3-Ni/Al_2O_3/CNCs, hereafter). The Ni/Al_2O_3/CNCs also exhibit good ability for microwave absorption. At the thickness of 1.5 mm, the minimum RL of 8.9-Ni/Al_2O_3/CNC is −14.7 dB at 13.5 GHz and the bandwidth corresponding to RL below −10 dB is higher than 3.6 GHz (Figure 6D).

CONCLUSION

In summary, we have demonstrated that it is feasible to prepare magnetic CNCs with conveniently and highly controlled multilayer structures and good conformality by ALD technology. The as-prepared magnetic CNCs show a much lower RL and wider absorption frequency range than those of pristine CNCs. The enhanced microwave absorption properties of magnetic CNCs arise from the efficient complementarity between complex permittivity and permeability, chiral morphology, and multilayer structure of the products. The carbon nanocoils coated with magnetic materials by ALD can be fabricated at large scales and are commercially feasible to be used as microwave absorbers since the production capacity can be greatly increased by applying batch reactors with large reactor volume.[8] Considering the vast library of magnetic materials and high dielectric materials available by ALD, application of ALD technology to prepare hybrid nanomaterials and adjust materials' complex permittivity and permeability would be very promising to design excellent microwave absorbers.

METHODS

Experimental Procedure. The CNCs used in this work were synthesized by chemical vapor deposition using acetylene as a carbon source and copper nanoparticles as catalysts at 250 °C followed by a heat treatment at 900 °C for 1 h as reported previously.[40] The ALD process was carried out in a hot-wall closed chamber-type ALD reactor. Prior to ALD, the CNCs were dispersed in ethanol by ultrasonic agitation and then dropped onto a quartz wafer. After being air-dried, an Al_2O_3 protection layer was first deposited by ALD at 200 °C using trimethylaluminum and water as the aluminum and oxygen source, respectively. Subsequently, the Fe_2O_3 or NiO coatings were deposited by sequential exposure of the nanocoils to ferrocene ($FeCp_2$) or nickelocene ($NiCp_2$) and O_3. Deposition temperatures for Fe_2O_3 and NiO were 250 and 150 °C, respectively. $FeCp_2$ and $NiCp_2$ were kept at 100 and 80 °C, respectively. Finally, after the ALD process, the samples were transferred to a furnace and reduced at 450 °C in 5% H_2/N_2 atmosphere for 2 h.

Characterization of the Samples. The XRD patterns were collected on a Bruker D8 Advance X-ray diffractometer. The TEM and HRTEM images were taken on a JEOL-2100F microscope. The composition of the samples was analyzed by EDX attached to the TEM instrument. The magnetic properties were measured using a MicroMag 2900/3900 alternating gradient magnetometer. The specimens for measuring the EM properties were prepared by uniformly mixing 25 wt % carbon nanocoils or coated nanocoils with paraffin and pressing the mixture into a cylindrical shape. Then the cylinder was cut into a toroid of 7.00 mm outer diameter and 3.04 mm inner diameter for measurement. The relative permeability and permittivity values of the mixture were determined between 2 and 18 GHz with an Agilent 8722ES network analyzer by using the transmission/reflection coaxial line method.

Conflict of Interest: The authors declare no competing financial interest.

Acknowledgment. This work was financially supported by National Natural Science Foundation of China (Grant No. 21173248) and in-house project of State Key Laboratory of Coal Conversion (No. Y1BWLI1991). S.W.T. and L.Z. acknowledge the financial support from National Natural Science Foundation of China (Grant Nos. 60990321 and 11174055) and Program of Shanghai Subject Chief Scientist (12XD1400700).

Supporting Information Available: Additional figures and experimental details are included. This material is available free of charge *via* the Internet at http://pubs.acs.org.

REFERENCES AND NOTES

1. Liao, S. B.; Yin, G. J. Reflectance of a Chiral Plate Absorber. *Appl. Phys. Lett.* **1993**, *62*, 2480–2482.
2. Rogacheva, A. V.; Fedotov, V. A.; Schwanecke, A. S.; Zheludev, N. I. Giant Gyrotropy Due to Electromagnetic-Field Coupling in a Bilayered Chiral Structure. *Phys. Rev. Lett.* **2006**, *97*, 177401.
3. Umari, M. H.; Varadan, V. K.; Varadanm, V. V. Rotation and Dichroism Associated with Microwave Propagation in Chiral Composite Samples. *Radio Sci.* **1991**, *2*, 1327–1334.
4. Gansel, J. K.; Thiel, M.; Rill, M. S.; Deker, M.; Bade, K.; Saile, V.; Freymann, G.; Linden, S.; Wegener, M. Gold Helix Photonic Metamaterial as Broadband Circular Polarizer. *Science* **2009**, *325*, 1513–1515.
5. Tang, N. J.; Zhong, W.; Au, C. T.; Gedanken, A.; Yang, Y.; Du, Y. W. Large-Scale Synthesis, Annealing, Purification, and Magnetic Properties of Crystalline Helical Carbon Nanotubes with Symmetrical Structures. *Adv. Funct. Mater.* **2007**, *17*, 1542–1550.
6. Tang, N. J.; Wen, J. F.; Zhang, Y.; Liu, F. X.; Lin, K. J.; Du, Y. W. Helical Carbon Nanotubes: Catalytic Particle Size-Dependent Growth and Magnetic Properties. *ACS Nano* **2010**, *4*, 241–250.
7. Xie, G. W.; Wang, Z. B.; Cui, Z. L.; Shi, Y. L. Ni-Fe-Co-P Coatings on Coiled Carbon Nanofibers. *Carbon* **2005**, *43*, 3183–3183.
8. George, S. M. Atomic Layer Deposition: An Overview. *Chem. Rev.* **2010**, *110*, 111–131.
9. Knez, M.; Nielsch, K.; Niinistö, L. Synthesis and Surface Engineering of Complex Nanostructures by Atomic Layer Deposition. *Adv. Mater.* **2007**, *19*, 3425–3438.
10. Marichy, C.; Bechelany, M.; Pinna, N. Atomic Layer Deposition of Nanostructured Materials for Energy and Environmental Applications. *Adv. Mater.* **2012**, *24*, 1017–1032.
11. Groner, M. D.; Fabreguette, F. H.; Elam, J. W.; George, S. M. Low-Temperature Al_2O_3 Atomic Layer Deposition. *Chem. Mater.* **2004**, *16*, 639–645.
12. Ritala, M.; Leskelä, M. Zirconium Dioxide Thin Films Deposited by ALE Using Zirconium Tetrachloride as Precursor. *Appl. Surf. Sci.* **1994**, *75*, 333–340.
13. Bachmanm, J.; Jing, J.; Knez, M.; Barth, S.; Shen, H.; Mathur, S.; Gösele, U.; Nielsch, K. Ordered Iron Oxide Nanotube Arrays of Controlled Geometry and Tunable Magnetism by Atomic Layer Deposition. *J. Am. Chem. Soc.* **2007**, *129*, 9554–9555.
14. Kim, W. H.; Lee, H. B. R.; Heo, K.; Lee, Y. K.; Chung, T. M.; Kim, C. G.; Hong, S.; Heo, J.; Kim, H. Atomic Layer Deposition of Ni Thin Films and Application to Area-Selective Deposition. *J. Electrochem. Soc.* **2011**, *158*, D1–D5.
15. Lee, H. B. R.; Gu, G. H.; Son, J. Y.; Park, C. G.; Kim, H. Spontaneous Formation of Vertical Magnetic-Metal-Nanorod Arrays during Plasma-Enhanced Atomic Layer Deposition. *Small* **2008**, *4*, 2247–2254.
16. Daub, M.; Knez, M.; Goesele, U.; Nielsch, K. Ferromagnetic Nanotubes by Atomic Layer Deposition in Anodic Alumina Membranes. *J. Appl. Phys.* **2007**, *101*, 09J111.
17. Chong, Y. T.; Yau, E. M. Y.; Nielsch, K.; Bachmann, J. Direct Atomic Layer Deposition of Ternary Ferrites with Various Magnetic Properties. *Chem. Mater.* **2010**, *22*, 6506–6508.
18. Escrig, J.; Bachmann, J.; Jing, J.; Daub, M.; Altbir, D.; Nielsch, K. Crossover between Two Different Magnetization Reversal Modes in Arrays of Iron Oxide Nanotubes. *Phys. Rev. B* **2008**, *77*, 214421.

19. Martinson, A. B. F.; DeVries, M. J.; Libera, J. A.; Christensen, S. T.; Hupp, J. T.; Pellin, M. J.; Elam, J. W. Atomic Layer Deposition of Fe_2O_3 Using Ferrocene and Ozone. *J. Phys. Chem. C* **2011**, *115*, 4333–4339.
20. Bachmann, J.; Escrig, J.; Pitzschel, K.; Moreno, J. M. M.; Jing, J.; Görlitz, D.; Altbir, D.; Nielsch, K. Size Effects in Ordered Arrays of Magnetic Nanotubes: Pick Your Reversal Mode. *J. Appl. Phys.* **2009**, *105*, 07B521.
21. Roy, A. K.; Schulze, S.; Hietschold, M.; Goedel, W. A. Oxidation Protection of Carbon Fibers by Coating with Alumina and/or Titania Using Atomic Layer Deposition. *Carbon* **2012**, *50*, 761–770.
22. Lie, M.; Fjellvag, H.; Kjekshus, A. Growth of Fe_2O_3 Thin Films by Atomic Layer Deposition. *Thin Solid Films* **2005**, *488*, 74–81.
23. Nicolson, A. M.; Ross, G. Measurement of the Intrinsic Properties of Materials by Time Domain Techniques. *IEEE Trans. Instrum. Meas.* **1970**, *19*, 377–382.
24. Weir, W. B. Automatic Measurement of Complex Dielectric Constant and Permeability at Microwave Frequencies. *Proc. IEEE* **1974**, *62*, 33–36.
25. Naito, Y.; Suetake, K. Application of Ferrite to Electromagnetic Wave Absorber and Its Characteristics. *IEEE Trans. Microwave Theory Tech.* **1971**, *19*, 65–72.
26. Kim, S. S.; Jo, S. B.; Gueon, K. I.; Choi, K. K.; Kim, J. M.; Churn, K. S. Complex Permeability and Permittivity and Microwave Absorption of Ferrite-Rubber Composite in X-Band Frequencies. *IEEE Trans. Magn.* **1991**, *27*, 5462–5464.
27. Che, R. C.; Duan, X. F.; Chen, Q.; Liang, X. L.; Peng, L. M. Microwave Absorption Enhancement and Complex Permittivity and Permeability of Fe Encapsulated within Carbon Nanotubes. *Adv. Mater.* **2004**, *16*, 401–405.
28. Liu, J. R.; Itoh, M.; Machida, K. Electromagnetic Wave Absorption Properties of α-Fe/Fe_3B/Y_2O_3 Nanocomposites in Gigahertz Range. *Appl. Phys. Lett.* **2003**, *83*, 4017–4019.
29. Xu, P.; Han, X. J.; Wang, C.; Zhou, D. H.; Lv, Z. S.; Wen, A. H.; Wang, X. H.; Zhang, B. Synthesis of Electromagnetic Functionalized Nickel/Polypyrrole Core/Shell Composites. *J. Phys. Chem. B* **2008**, *112*, 10443–10448.
30. Liu, J. R.; Itoh, M.; Machida, K. I. Magnetic and Electromagnetic Wave Absorption Properties of α-Fe/Z-Type Ba-Ferrite Nanocomposites. *Appl. Phys. Lett.* **2006**, *88*, 62503.
31. Zhang, X. F.; Dong, X. L.; Huang, H.; Liu, Y. Y.; Wang, W. N.; Zhu, X. G.; Lv, B.; Lei, J. P.; Lee, C. G. Microwave Absorption Properties of the Carbon-Coated Nickel Nanocapsules. *Appl. Phys. Lett.* **2006**, *89*, 53115.
32. Motojima, S.; Hoshiya, S.; Hishikawa, Y. Electromagnetic Wave Absorption Properties of Carbon Microcoils/PMMA Composite Beads in W Bands. *Carbon* **2003**, *41*, 2653–2689.
33. Pendry, J. B. A Chiral Route to Negative Refraction. *Science* **2004**, *306*, 1353–1355.
34. Chen, Y. J.; Xiao, G.; Wang, T. S.; Ouyang, Q. Y.; Qi, L. H.; Ma, Y.; Gao, P.; Zhu, C. L.; Cao, M. S.; Jin, H. B. Porous Fe_3O_4/Carbon Core/Shell Nanorods: Synthesis and Electromagnetic Properties. *J. Phys. Chem. C* **2011**, *115*, 13603–13608.
35. Cao, J.; Fu, W.; Yang, H. B.; Yu, Q. J.; Zhang, Y. Y.; Liu, S. K.; Sun, P.; Zhou, X. M.; Leng, Y.; Wang, S. M.; Liu, B. B.; Zou, G. T. Large-Scale Synthesis and Microwave Absorption Enhancement of Actinomorphic Tubular ZnO/$CoFe_2O_4$ Nanocomposites. *J. Phys. Chem. B* **2009**, *113*, 4642–4647.
36. Ohlan, A.; Singh, K.; Chandra, A.; Dhawan, S. K. Microwave Absorption Behavior of Core−Shell Structured Poly(3,4-ethylenedioxy thiophene)-Barium Ferrite Nanocomposites. *ACS Appl. Mater. Interfaces* **2010**, *2*, 927–933.
37. Liu, J. W.; Che, R. C.; Chen, H. J.; Zhang, F.; Xia, F.; Wu, Q. S.; Wang, M. Microwave Absorption Enhancement of Multifunctional Composite Microspheres with Spinel Fe_3O_4 Cores and Anatase TiO_2 Shells. *Small* **2012**, *8*, 1214–1221.
38. Liu, X. G.; Qu, Z. Q.; Geng, D. Y.; Han, Z.; Jiang, J. J.; Liu, W.; Zhang, Z. D. Influence of a Graphite Shell on the Thermal and Electromagnetic Characteristics of FeNi Nanoparticles. *Carbon* **2010**, *48*, 891–897.
39. Zhu, J. H.; Wei, S. Y.; Haldolaarachchige, N.; Young, D. P.; Guo, Z. H. Electromagnetic Field Shielding Polyurethane Nanocomposites Reinforced with Core−Shell Fe-Silica Nanoparticles. *J. Phys. Chem. C* **2011**, *115*, 15304–15310.
40. Qin, Y.; Zhang, Z. K.; Cui, Z. L. Helical Carbon Nanofibers Prepared by Pyrolysis of Acetylene with a Catalyst Derived from the Decomposition of Copper Tartrate. *Carbon* **2003**, *41*, 3072–3074.
41. Qin, Y.; Zhang, Z. K.; Cui, Z. L. Helical Carbon Nanofibers with a Symmetric Growth Mode. *Carbon* **2004**, *42*, 1917–1922.
42. Guerin, F. Microwave Chiral Materials: A Review of Experimental Studies and Some Results on Composites with Ferroelectric Ceramic Inclusions. *Prog. Electromαgn. Res.* **1994**, *Pier 9*, 219–263.